

Phase Structure of QCD Matter in a Chiral Effective Model with Quarks

Philip Rau,^{1,2,*} Jan Steinheimer,² and Stefan Schramm^{1,2}

¹*Institut für Theoretische Physik, Goethe Universität,
Max-von-Laue-Str. 1, 60438 Frankfurt am Main, Germany*

²*Frankfurt Institute for Advanced Studies (FIAS),
Ruth-Moufang-Str. 1, 60438 Frankfurt am Main, Germany*

Using a unified hadron-quark effective model for the QCD equation of state, this paper studies the phase structure of strongly interacting matter in a wide range of temperature and baryonchemical potential. At small potentials the model yields a smooth cross-over to chirally restored matter with a transition temperature and curvature in line with recent lattice QCD estimates and thermal model fits of freeze-out curves. Trajectories of constant entropy per net baryon number show a clear dependence on the particle composition in the model and on repulsive vector field interactions. Although the model might feature a critical end-point at a rather high baryonchemical potential and low temperature, probing it in heavy-ion collisions might be highly challenging due to a large thermodynamic spread of matter in the collision fireball.

PACS numbers: 12.38.-t, 11.30.Rd, 25.75.Nq, 21.65.Mn

INTRODUCTION

A main objective in studying relativistic heavy-ion collisions lies in investigating the behavior of strongly-interacting matter under extreme conditions, i.e. high temperatures T and baryon densities ρ_B . Particularly focusing on the phase structure and on mapping the phase transitions to chirally restored and deconfined matter in the QCD phase diagram. Experimentally this can be accomplished by studying observables for the phase transition at different beam energies corresponding to different excitation energies and baryon densities. While results from high-energy collisions at RHIC suggest the existence of a quark-gluon plasma (QGP) at high T and small μ_B [1, 2], the QCD phase structure in other regions (i.e. $\mu_B > 0$) remains largely unknown. Searching for transition signatures by scanning a range of beam energies was part of the SPS program [3], is currently performed at RHIC [4], and will also be a key objective of the CBM experiment at FAIR [5].

At $\mu_B = 0$ lattice QCD consistently shows a smooth cross-over transition with a “critical” temperature $T_c \approx 155$ MeV [6, 7]. At $\mu_B > 0$ lattice QCD standard lattice QCD methods fail due to the fermion sign problem and estimates from extrapolation are ambiguous. While older results suggest a critical end-point (CEP) with shift from a smooth cross-over to a first-order phase transition at finite μ_B [8–10], more recent continuum extrapolated lattice estimates do not necessarily show a first order phase transition [11]. So far there are no experimental indications for a CEP to exist.

Further information on the phase structure of QCD matter is provided by effective models such as pure quark Polyakov-loop extended Nambu-Jona-Lasinio (PNJL) models [12–16] or Polyakov-quark-meson (PQM) models [17–20]. However, since in these models the Polyakov loop potentials are fixed at vanishing μ_B [17], their va-

lidity for describing QCD matter decreases with higher potentials and baryon densities. To the disadvantage of these models, in the high- μ_B region, baryon densities become large and baryon resonances may exhibit high multiplicities and tend to affect the phase structure significantly [21]. To circumvent these restraints, in this work the QCD phase structure is studied using a unified chiral effective model which combines hadron and quark degrees of freedom in a single partition function and provides the correct degrees of freedom in a wide range of T and μ_B .

MODEL

This study of the QCD phase structure uses a chiral SU(3)-flavor σ - ω model [22–26] for describing the hadronic phase and a PNJL-type approach for quarks; see [26] for a detailed review of the model and all parameters. Particles in the model include all baryons from the octet, the decuplet and all known resonances with $m \leq 2.6$ GeV [27], as well as the full set of scalar, pseudoscalar, vector, and axial vector mesons including all meson resonance states. Additionally, the three lightest quark flavors (u , d , s) are included. The fields are treated in mean field approximation and correspond to the chiral quark condensates, i.e. the scalar σ , its strange counterpart ζ , and the vector ω and ϕ fields. The interaction between particles and fields is described by

$$\mathcal{L}_{\text{int}} = - \sum_i \bar{\psi}_i [\gamma_0 (g_{i\omega}\omega^0 + g_{i\phi}\phi^0) + m_i^*] \psi_i, \quad (1)$$

with i running over all baryons and quarks. Scalar field couplings $g_{i\sigma,\zeta}$ dynamically generate the effective masses

$$m_i^* = g_{i\sigma}\sigma + g_{i\zeta}\zeta + \delta m_i, \quad (2)$$

except for a small explicit mass δm_i ($\delta m_{u,d} = 6$ MeV, $\delta m_s = 105$ MeV for quarks and $\delta m_{n,p} = 150$ MeV for nucleons). The dynamic mass generation ensures decreasing

masses with higher T and μ_B and, thus, the restoration of chiral symmetry. The vector couplings $g_{i\omega,\phi}$ generate the effective chemical potentials accordingly

$$\mu_i^* = \mu_i - g_{i\omega}\omega - g_{i\phi}\phi. \quad (3)$$

Using the notation $X = \sigma^2 + \zeta^2$, the scalar meson self-interactions are introduced as

$$\begin{aligned} \mathcal{L}_{\text{scal}} = & -\frac{1}{2}k_0 X + k_1 X^2 + k_2 \left(\frac{\sigma^4}{2} + \zeta^4 \right) + k_3 \sigma^2 \zeta \\ & - k_4 \chi^4 - \frac{1}{4} \chi^4 \ln \frac{\chi^4}{\chi_0^4} + \frac{\delta}{3} \chi^4 \ln \frac{\sigma^2 \zeta}{\sigma_0^2 \zeta_0}, \end{aligned} \quad (4)$$

with the last two terms describing QCD trace anomaly by introducing the gluon condensate χ (dilaton field) [24]. The vector meson self-interactions are given by

$$\begin{aligned} \mathcal{L}_{\text{vec}} = & \frac{1}{2} \frac{\chi}{\chi_0} (m_\omega^2 \omega^2 + m_\phi^2 \phi^2) \\ & + g_4 \left(\omega^4 + \frac{\phi^4}{4} + 3\omega^2 \phi^2 + \frac{4\omega^3 \phi}{\sqrt{2}} + \frac{2\omega \phi^3}{\sqrt{2}} \right) \end{aligned} \quad (5)$$

and the explicit breaking of chiral symmetry due to non-zero current quark masses adds the following terms to the Lagrangian

$$\mathcal{L}_{\text{SB}} = -\frac{\chi^2}{\chi_0^2} \left[m_\pi^2 f_\pi \sigma + \left(\sqrt{2} m_k^2 f_k - \frac{1}{\sqrt{2}} m_\pi^2 f_\pi \right) \zeta \right]. \quad (6)$$

The baryon couplings to the fields are fixed such as to reproduce nuclear saturation properties and vacuum masses [23, 24] and the quark couplings are chosen according to the additive quark model and to avoid free quarks from appearing in the ground state. All baryon resonance couplings are scaled to the respective nucleon couplings via $g_{B_i\sigma,\zeta} = r_s g_{N\sigma,\zeta}$ and $g_{B_i\omega,\phi} = r_v g_{N\omega,\phi}$ [21]. While the scalar coupling stays $r_s \approx 1$ to obtain a smooth cross-over at $\mu_B = 0$, the vector coupling r_v is a free parameter. The repulsive effect of the vector couplings controls the particle abundances at finite μ_B (Eq. (3)) and, thus, has large impact on the resulting phase structure. In the hadron sector, reasonably large vector couplings ($r_v \approx 1$) cause the disappearance of a first-order phase transition but yield a smooth cross-over transition due to the gradual appearance of baryon resonances with higher T and μ_B [21]. In contrast, all quark vector couplings have to vanish in order not to fully quench baryon number fluctuations in the transition region [28].

Quarks are introduced as in PNJL models, defining the scalar Polyakov loop field Φ by tracing the time component A_0 of the SU(3) color gauge field $\Phi = 1/3 \text{Tr} [\exp(-A_0/T)]$. For static quark masses, Φ is an order parameter for deconfinement indicating the breakdown of Z(3) center symmetry. The effective Polyakov loop potential

$$\begin{aligned} U = & - (a(T)\bar{\Phi}\Phi) / 2 + b (T_0/T)^3 \ln [1 - 6\bar{\Phi}\Phi \\ & + 4(\bar{\Phi}^3 + \Phi^3) - 3(\bar{\Phi}\Phi)^2], \end{aligned} \quad (7)$$

with $a(T) = a_0 + a_1 (T_0/T) + a_2 (T_0/T)^2$ and the critical Polyakov temperature T_0 is taken from [29]. It enters the grand canonical potential and controls the transition from hadrons to quarks. It is constructed such as to reproduce quenched lattice QCD thermodynamics and known features of the deconfinement transition [29]. In the confined phase, the minimum of $U(T, \Phi, \bar{\Phi})$ is located at $\Phi = 0$ and it moves towards $\Phi \rightarrow 1$ with increasing T . Furthermore, Φ couples to the dilaton field

$$\chi = \chi_0 \left[1 - 1/4 (\Phi^2 + \bar{\Phi}^2)^2 \right] \quad (8)$$

to suppress the chiral condensate in the quark phase.

All thermodynamic quantities are derived from the grand canonical potential

$$\Omega/V = -\mathcal{L}_{\text{int}} - \mathcal{L}_{\text{mes}} + \Omega_{\text{th}}/V - U_{\text{Pol}}, \quad (9)$$

with Ω_{th} including thermal contributions from mesons, baryons, and quarks ($j = u, d, s$) in the form

$$\begin{aligned} \Omega_{\text{q}\bar{\text{q}}} = & -T \sum_j \frac{\gamma_j}{(2\pi)^3} \int d^3k \left(\ln \left[1 + \Phi e^{-\frac{1}{T}(E_j^*(k) - \mu_j^*)} \right] \right. \\ & \left. + \ln \left[1 + \bar{\Phi} e^{-\frac{1}{T}(E_j^*(k) + \mu_j^*)} \right] \right), \end{aligned} \quad (10)$$

with the spin-isospin degeneracy factor γ_j , and the single particle energy $E_j^*(k) = (k^2 + m_j^{*2})^{1/2}$. By minimizing $\Omega/V(T, \mu)$ with respect to the fields one obtains the self-consistent equations of motion for fields and particle densities. From these, thermodynamic variables are derived via the pressure $p = -\partial\Omega/\partial V$, the entropy density $s = \partial p/\partial T$, and the energy density $\varepsilon = Ts - pV + \sum_i \mu_i \rho_i$.

A shift in the degrees of freedom from a hadron resonance gas (HRG) at low T and ρ_B to a pure quark gas in the the high- T , high- ρ region is attained by including an eigenvolume V_{ex}^i for hadrons [30–32]. The baryon V_{ex}^B is chosen according to the proton charge radius [33], mesons are assumed to exhibit half of this radius, and quarks remain point-like. At high T and μ , when quark multiplicities rise quickly, this formalism suppresses hadrons and establishes the shift to a pure quark phase. Thermodynamic consistency is preserved by redefining μ_i^* , i.e. reducing it by the occupied volume [26], and multiply the particle densities ρ_i as well as ε and s with a correction factor given by the ratio of the total volume to the non-occupied sub-volume.

RESULTS

The chiral transition extracted from the hadron sector of the model [21] (black line in Fig. 1) can be parametrized analog to a lattice QCD estimate [34] by

$$T_c(\mu_B) = T_0 \left(1 - 0.0193 \left(\frac{\mu_B}{T_0} \right)^2 \right) \quad (11)$$

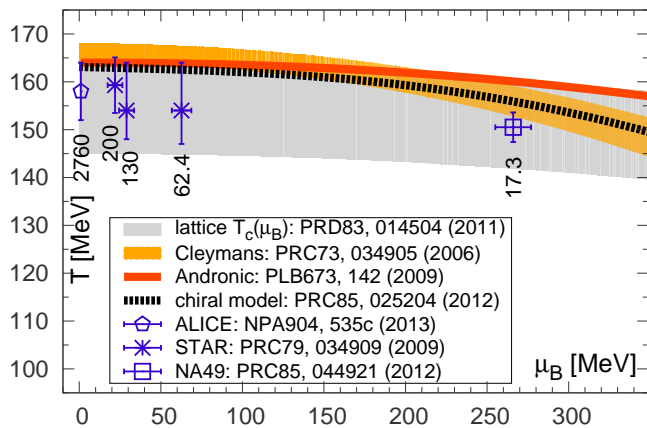


Figure 1. Chiral transition at small μ_B from lattice QCD [34, 35] (gray band) and from the chiral model [21] (black line) contrasted to freeze-out curves from statistical and thermal model fits [36–41] for SPS to LHC energies ($\sqrt{s_{NN}}$ in GeV).

with $T_0 = T_c(\mu_B = 0) = 164$ MeV. In the chiral model this curve is extracted at the point of the steepest decrease in $\sigma(T)$ at a given baryonchemical potential. The curve agrees well with different models and experimental results at different beam energies. In [42] a constant value of the interaction measure $(e - 3p)/T^4 = 7/2$ was proposed to reliably parametrize the chemical freeze-out curve. This parametrization can be reproduced in the hadronic sector of the chiral model. However, since in the chiral transition region the interaction measure increases very fast with higher T , other constant values of $(e - 3p)/T^4$ close to $7/2$ also yield curves close to recent freeze-out parametrizations. In general, the transition behavior is not affected by additionally taking into account the quark phase. Even in the presence of a quark phase, baryon multiplicities at the chiral transition are high and the steepest decline in σ still takes place in the HRG. But when considering quarks, T_c is shifted to slightly higher values [26]. For this reason, and due to the non-existence of direct coupling effects between Φ and the quark condensates, quarks have only minor impact on the critical temperature of the chiral transition.

In [43] it is shown that, using a fixed target setup, highest net baryon number densities at freeze-out can be achieved in heavy-ion collisions at energies close to $E_{lab} = 30$ A GeV. Accelerators at the upcoming FAIR facility, operating between 5 and 40 GeV per nucleon, will cover this energy range. Figure 2 and 3 show the isentropic expansion paths, i.e. lines of constant entropy per net baryon number S/A , corresponding to these collision energies. The adiabats are depicted in the hadronic equation of state (EoS) without a quark phase and feature two values for the resonance vector couplings. In case of a rather weak coupling $r_v = 0.4$ (Fig. 2) the phase structure exhibits a first order phase transition up to $T \approx 60$ MeV, an adjacent CEP, and a smooth

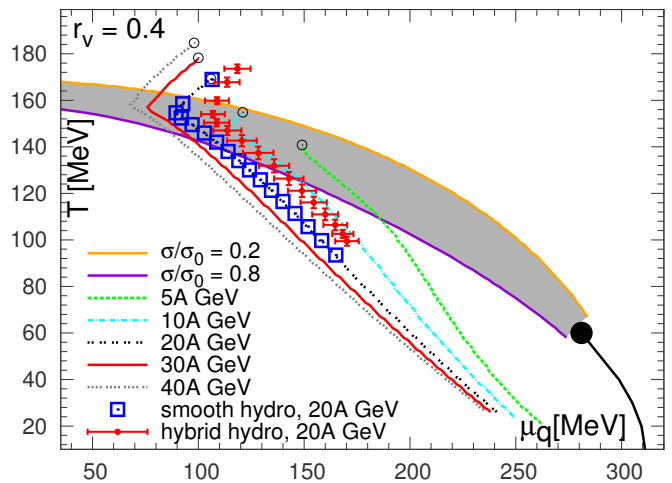


Figure 2. Isentropic expansion paths (lines of constant S/A) for different E_{lab} in the T - μ_q -plane of the pure hadron EoS ($r_v = 0.4$) together with lines of constant σ/σ_0 and the first-order phase transition with a CEP (black solid line). Red points depict the central cell in the UrQMD hybrid model (Au+Au at $E_{lab} = 20$ A GeV, averaged over 400 events) and blue squares illustrate a smooth hydrodynamic evolution with a time interval of 1 fm between the data points.

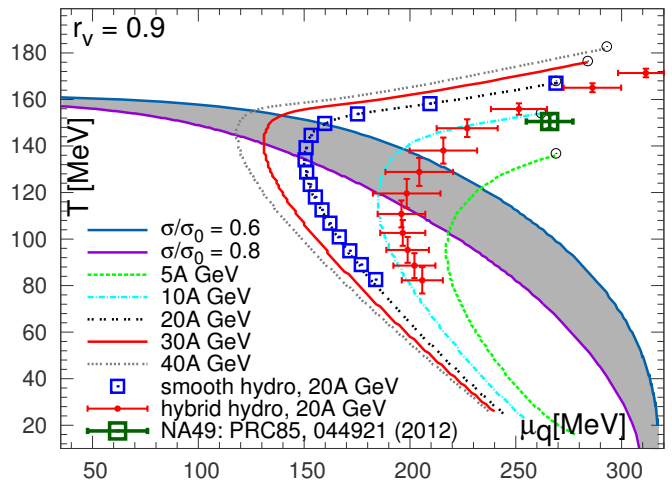


Figure 3. Adiabats as in Fig.2 using a larger resonance vector coupling $r_v = 0.9$, for which no first order phase transition exists. The green marker depicts the freeze-out point extracted from NA49 data [40] (cf. Fig. 1).

but rapid cross-over transition for higher temperatures (gray band). In the transition region, with increasing T , the rapid incline in m_i^* of the baryons induces large baryon multiplicities and a sharply rising energy density and pressure along the μ_q -axis (i.e. $\mu_q = \mu_B/3$) causing the adiabats to bend sharply at the chiral transition distant to the CEP.

This behavior changes for more reasonable resonance vector couplings $r_v = 0.9$ (Fig. 3) for which the changes in ε and p are much slower along the μ_q -axis and the chiral transition takes place in a much broader T -range

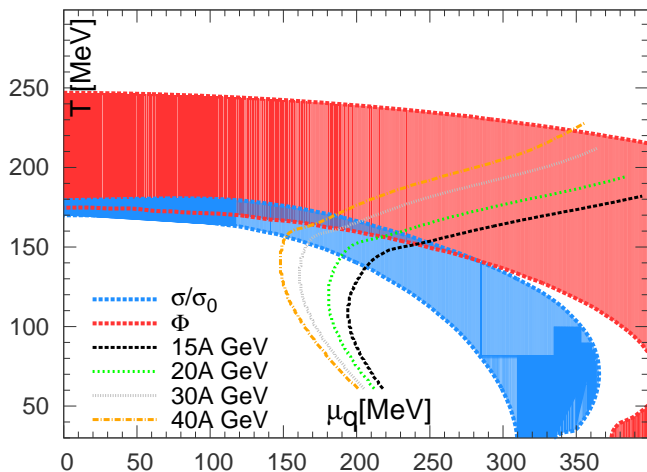


Figure 4. Order parameter σ/σ_0 (blue) and Φ (red) of the effective model including hadrons and quarks along with isentropic adiabats. In the colored areas σ/σ_0 declines from 0.7 to 0.4 and Φ rises from 0.7 to 0.4 with increasing T and μ_q . The vector couplings are $g_{q\omega} = 0$ for quarks and $r_v = 0.9$ for baryon resonances.

due suppressive vector field interactions. In this case, neither a first order phase transition nor a CEP exists and the chiral transition takes place in a much broader T -range. Compared to $r_v = 0.4$, substantial softening of the EoS with larger r_v causes the adiabats to smoothly bend at the chiral transition and to reach notably higher μ_q while the initial T only changes on a minor scale.

The figures also depict dynamic expansion paths of the fireball at 20A GeV from ideal hydrodynamics [44] using initial densities from a geometric overlap model [45] (blue squares). Also shown are collision dynamics from the UrQMD hybrid model with fluctuating initial conditions [46] (red crosses) sampling over the central cell in 400 Au+Au collisions with a time interval of $\Delta t = 1$ fm between data points. In case of a soft EoS (Fig. 3), initial fluctuations cause a larger dispersion in T and μ on an event-by-event basis. Furthermore, initial state density fluctuations create sub-regions in the fireball and cause a notable dispersion of the thermodynamic properties of the fireball matter. Due to this effect, QCD matter may spread over at least 50 MeV in μ_q in each single event [47]. This means that there is no well defined and narrow isentropic adiabat corresponding to a single event and energy but rather a large area of the phase diagram is covered in one collision at a specific energy. While on the one hand, this eventually allows for probing regions well outside a narrow adiabat, on the other hand poses the question of how to map back final state observables to matter properties to one specific point in T and μ on the QCD phase diagram.

Additionally including quarks (Fig. 4 using $g_{q\omega} = 0$) has only minor effect on the adiabat curvature at the chiral transition. However, in the presence of a quark

phase, the adiabats are slightly steeper in the chiral limit and higher initial T and μ_q are achieved. In close analogy to the effect of the vector coupling of resonances r_v in the purely hadronic EoS, turning up the quark vector coupling $g_{q\omega}$ from zero to finite values, causes significantly higher initial values in μ_q and almost flat adiabat curvatures above the chiral transition in the full model including quarks.

SUMMARY

In summary, using an effective model with hadrons and quarks, we present a parametrization for the chiral transition at small μ_B agreeing well with other recent results on this topic. Isentropic adiabats in the EoS are discussed in the context of varying vector interactions: Probing the CEP and a first order phase transition at FAIR energies might be difficult due to the distance of isentropic adiabats to the first order phase transition in the model. Additionally, probing specific points in the QCD phase diagram may be even more complicated considering the sizable thermodynamic spread of fireball matter induced by initial state fluctuations as seen in dynamic models for heavy-ion collisions.

ACKNOWLEDGEMENTS

This work was supported by BMBF, GSI, and the Hessian LOEWE initiative through the Helmholtz International Center for FAIR and the Helmholtz Graduate School for Hadron and Ion Research. Computing resources were provided by the Center for Scientific Computing of the Goethe University Frankfurt.

* rau@th.physik.uni-frankfurt.de

- [1] J. Adams et al., Nucl. Phys. **A757**, 102 (2005).
- [2] K. Adcox et al., Nucl. Phys. **A757**, 184 (2005).
- [3] C. Alt et al. (NA49 Collaboration), Phys.Rev. **C77**, 024903 (2008).
- [4] S. Shi (STAR Collaboration), Nucl.Phys.A904-905 **2013**, 895c (2013).
- [5] C. Hohn, Nucl.Phys. **A830**, 369C (2009).
- [6] Y. Aoki, G. Endrodi, Z. Fodor, S. Katz, and K. Szabo, Nature **443**, 675 (2006).
- [7] M. Cheng et al., Phys. Rev. **D74**, 054507 (2006).
- [8] A. M. Halasz, A. Jackson, R. Shrock, M. A. Stephanov, and J. Verbaarschot, Phys.Rev. **D58**, 096007 (1998).
- [9] P. de Forcrand and O. Philipsen, Nucl. Phys. **B673**, 170 (2003).
- [10] Z. Fodor and S. D. Katz, JHEP **04**, 050 (2004).
- [11] S. Borsanyi, G. Endrodi, Z. Fodor, S. Katz, S. Krieg, et al., JHEP **1208**, 053 (2012).
- [12] K. Fukushima, Phys.Lett. **B591**, 277 (2003).

- [13] P. N. Meisinger and M. C. Ogilvie, Nucl.Phys.Proc.Suppl. **47**, 519 (1996).
- [14] C. Ratti, M. Thaler, and W. Weise, Rom.Rep.Phys. **58**, 13 (2006).
- [15] C. Ratti, M. A. Thaler, and W. Weise (2006), arXiv:nucl-th/0604025.
- [16] S. Roessner, C. Ratti, and W. Weise, Phys.Rev. **D75**, 034007 (2006).
- [17] B.-J. Schaefer, J. M. Pawłowski, and J. Wambach, Phys.Rev. **D76**, 074023 (2007).
- [18] T. K. Herbst, J. M. Pawłowski, and B.-J. Schaefer, Phys.Lett. **B696**, 58 (2011).
- [19] V. Skokov, B. Stokic, B. Friman, and K. Redlich, Phys.Rev. **C82**, 015206 (2010).
- [20] L. M. Haas, R. Stiele, J. Braun, J. M. Pawłowski, and J. Schaffner-Bielich, Phys.Rev. **D87**, 076004 (2013).
- [21] P. Rau, J. Steinheimer, S. Schramm, and H. Stöcker, Phys.Rev. **C85**, 025204 (2012).
- [22] J. Boguta and H. Stöcker, Phys.Lett. **B120**, 289 (1983).
- [23] P. Papazoglou, S. Schramm, J. Schaffner-Bielich, H. Stöcker, and W. Greiner, Phys.Rev. **C57**, 2576 (1998).
- [24] P. Papazoglou, D. Zschesche, S. Schramm, J. Schaffner-Bielich, H. Stöcker, et al., Phys.Rev. **C59**, 411 (1999).
- [25] V. Dexheimer and S. Schramm, Astrophys.J. **683**, 943 (2008).
- [26] P. Rau, J. Steinheimer, S. Schramm, and H. Stöcker, J.Phys. **G40**, 085001 (2013).
- [27] J. Beringer et al. (Particle Data Group), Phys.Rev. **D86**, 010001 (2012).
- [28] P. Rau, J. Steinheimer, S. Schramm, and H. Stöcker (2013), arXiv:1308.4319 (hep-ph).
- [29] C. Ratti, S. Roessner, M. Thaler, and W. Weise, Eur.Phys.J. **C49**, 213 (2007).
- [30] D. H. Rischke, M. I. Gorenstein, H. Stöcker, and W. Greiner, Z. Phys. **C51**, 485 (1991).
- [31] J. Cleymans, J. Stalnacke, M. I. Gorenstein, and E. Suhonen, Phys.Scripta **48**, 277 (1992).
- [32] J. Steinheimer, S. Schramm, and H. Stöcker, J.Phys.G **G38**, 035001 (2011).
- [33] P. Mohr, B. Taylor, and D. Newell, *CODATA values of fundamental constants*, <http://physics.nist.gov/constants> (2011).
- [34] O. Kaczmarek et al., Phys. Rev. **D83**, 014504 (2011).
- [35] A. Bazavov, T. Bhattacharya, M. Cheng, C. DeTar, H. Ding, et al., Phys.Rev. **D85**, 054503 (2012).
- [36] J. Cleymans, H. Oeschler, K. Redlich, and S. Wheaton, Phys. Rev. **C73** (2006).
- [37] D. Zschesche, G. Zeeb, and S. Schramm, J.Phys. **G34**, 1665 (2007).
- [38] A. Andronic, P. Braun-Munzinger, and J. Stachel, Phys. Lett. **B673**, 142 (2009).
- [39] B. Abelev et al. (STAR Collaboration), Phys.Rev. **C79**, 034909 (2009).
- [40] F. Becattini, M. Bleicher, T. Kollegger, M. Mitrovski, T. Schuster, and R. Stock, Phys. Rev. **C85** (2012).
- [41] A. Andronic, P. Braun-Munzinger, K. Redlich, and J. Stachel, Nucl.Phys.A904-905 **2013**, 535c (2013).
- [42] A. Tawfik (2013), arXiv:1308.1712 (hep-ph).
- [43] J. Randrup and J. Cleymans, Phys.Rev. **C74**, 047901 (2006).
- [44] D. H. Rischke, S. Bernard, and J. A. Maruhn, Nucl.Phys. **A595**, 346 (1995).
- [45] M. Reiter, A. Dumitru, J. Brachmann, J. Maruhn, H. Stoecker, et al., Nucl.Phys. **A643**, 99 (1998).
- [46] H. Petersen, J. Steinheimer, G. Baur, M. Bleicher, and H. Stoecker, Phys.Rev. **C78**, 044901 (2008).
- [47] S. A. Bass, H. Petersen, C. Quammen, H. Canary, C. G. Healey, et al., Central Eur.J.Phys. **10**, 1278 (2012).